International Journal of GEOMATE, April, 2017, Vol. 12, Issue 32, pp. 63-69
Geotec., Const. Mat. & Env., ISSN:2186-2990, Japan, DOI: http://dx.doi.org/10.21660/2017.32.6610

AIR PRESSURE DISTRIBUTION INDUCED BY RAINFALL INFILTRATION IN SOIL/WATER/AIR COUPLED SIMULATION

*Katsuyuki KAWAI[1], Takuya KAWAKATSU[2] and Ayumi TERAOKA[1]

[1]Dept. Of Civil and Environmental Engineering, Kindai University, Japan; [2] Shimizu Corporation, Japan

*Corresponding Author, Received: 10 June 2016, Revised: 14 July 2016, Accepted: 21 Nov. 2016

ABSTRACT: Recently, the frequency of torrential rainfall has increased due to global climate change, and these events cause sediment potential failure. It is difficult to predict when and where a slope failure will occur because of the concentration of heavy rain. Knowing precursory phenomena, however, is effective for disaster reduction. Nonetheless, some of these phenomena have not been explained in the framework of geotechnical engineering. Organic smells and strange sounds, known as precursory signs of slope failure, propagate through the atmosphere. Therefore, it is important to monitor air movement within earth structures. This study focuses on pore air behavior within the ground due to rainfall infiltration. Here, the infiltration column test combined with monitoring smell, as conducted by Tsuchida et al., was first simulated using the soil/water/air coupled finite element code, DACSAR-MP. Next, a sloping earth structure exposed to rainfall was simulated. Consequently, it was found that distribution of pore air pressure was dependent on drainage conditions of air, and that pore air behavior influenced rainfall infiltration behavior.

Keywords: Unsaturated Soil, Soil/water/air Coupled Analysis, Slope Stability, Rainfall, Air Pressure

1. INTRODUCTION

Recently, torrential rainfall events have tended to occur locally, and it is difficult to predict damage from landslides due to rainfall. Therefore, increasing citizen awareness about disasters is needed to reduce disaster damage. In this regard, understanding precursory phenomena for landslides is effective. There are a lot of successful cases in which precursory phenomena acted as an alert. Because of this, precursory phenomena were introduced onto a hazard map published by Japanese government. However, some of these phenomena are difficult to explain theoretically in soil mechanics. In particular, the generating mechanism of unusual sound and smell before a landslide has not been clarified. These phenomena likely result from rainfall influencing air within the ground, since both sound and smell are transmitted by air. In this study, rainfall infiltration into sloped ground was simulated with soil/water/air coupled analysis to investigate localization of air within the ground.

2. PRIOR INVESTIGATIONS OF AIR BEHAVIOR WITHIN THE GROUND

Tsuchida et al. conducted soil column testing to investigate the relationship between rainfall infiltration and smell occurrence [1]. The soil column was installed with a profile moisture meter to measure the seepage line generated by a sprinkler fitted above the sandy soil column (Fig. 1). Smell was generated by a source at the bottom of the soil column, and leakage of smell from the surface of the soil column was measured with an odor intensity sensor. In this way, the distribution of the degree of saturation and odor intensity due to rainfall infiltration were monitored (shown in Fig. 2). First, it was found that degree of saturation started to increase from the bottom of the column, and the rise of the ground water level was more remarkable than the descent of the wetting front at the given rainfall condition. The odor intensity at the surface of the column drastically increased after an increase in the degree of saturation at each depth, a phenomena correlated to the rise of the groundwater level. Tsuchida et al. concluded that the groundwater level, determined by arriving to the bottom of infiltrated rain water, pushed air within the ground upwards, thus odor generation before a landslide signifies that the groundwater level is rising. However, their investigation was limited to one-dimensional infiltration. In this study, the soil column test performed by Tsuchida et al. was first simulated, followed by simulation of rainfall infiltration into virtual sloping ground.

3. SOIL/WATER/AIR COUPLED ANALYSIS

The soil/water/air coupled simulation code, DACSAR-MP [2], was used for rainfall simulation. The constitutive model for unsaturated soil, proposed by Ohno et al. [3], was adopted and

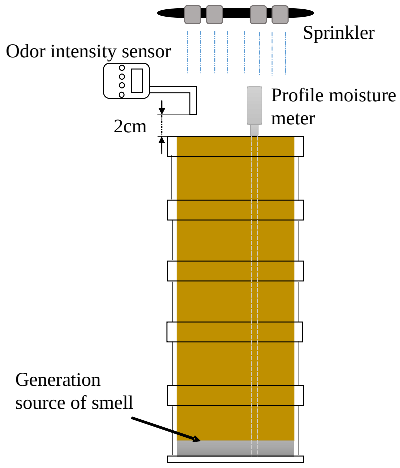

Fig. 1 Rainfall infiltration test by Tsuchida et al.

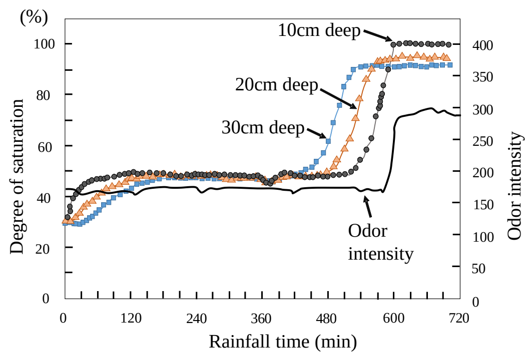

Fig. 2 Distribution of degree of saturation and odor intensity at the ground surface during rainfall

formulated with the theory of three phase's mixture material proposed by Borja [4].
In this way, effective stress is expressed as follows.

$$\boldsymbol{\sigma}' = \boldsymbol{\sigma}^{net} + p_s \mathbf{1} \tag{1}$$

$$\boldsymbol{\sigma}^{net} = \boldsymbol{\sigma} - p_a \mathbf{1}, \quad p_s = S_e s \tag{2}$$

$$s = p_a - p_w, \quad S_e = \frac{S_r - S_{rc}}{1 - S_{rc}} \tag{3}$$

Here, $\boldsymbol{\sigma}'$ is the effective stress tensor; $\boldsymbol{\sigma}^{net}$ is the net stress tensor; $\mathbf{1}$ is the second-order unit tensor; $\boldsymbol{\sigma}$ is the total stress tensor; s is suction; p_s is suction stress; p_a is pore air pressure; p_w is pore water pressure; S_r is degree of saturation; S_e is effective degree of saturation; and S_{rc} is degree of saturation at $s \to \infty$. The yield function is expressed as follows.

$$f\left(\boldsymbol{\sigma}', \zeta, \varepsilon_v^p\right) = MD \ln \frac{p'}{\zeta p'_{sat}} + \frac{MD}{n_E}\left(\frac{q}{Mp'}\right)^{n_E} - \varepsilon_v^p = 0 \tag{4}$$

$$\zeta = \exp\left[(1 - S_e)^{n_s} \ln a\right], \quad MD = \frac{\lambda - \kappa}{1 + e_0} \tag{5}$$

$$p' = \frac{1}{3}\boldsymbol{\sigma}' : \mathbf{1}, \; q = \sqrt{\frac{3}{2}\mathbf{s} : \mathbf{s}}, \; \mathbf{s} = \boldsymbol{\sigma}' - p'\mathbf{1} = \mathbf{A} : \boldsymbol{\sigma}', \; \mathbf{A} = \mathbf{I} - \frac{1}{3}\mathbf{1} \otimes \mathbf{1} \tag{6}$$

Here, n_E is a shaping parameter; ε_v^p is plastic volumetric strain; M is the stress ratio q/p' at the critical state; D is the dilatancy coefficient; p'_{sat} is the yield stress at saturated state; a and n_s are the parameters expressing the yield stress increment due to desaturation; and λ and κ are compression and expansion indices, respectively. Darcy's law is assumed for pore water and air flow as follows.

$$\tilde{\mathbf{v}}_\mathbf{w} = -\mathbf{k}_\mathbf{w} \cdot \mathrm{grad} h \tag{7}$$

$$\tilde{\mathbf{v}}_\mathbf{a} = -\mathbf{k}_\mathbf{a} \cdot \mathrm{grad} h_a, \; h_a = \frac{p_a}{\gamma_w} \tag{8}$$

Here, $\tilde{\mathbf{v}}_\mathbf{w}$ and $\tilde{\mathbf{v}}_\mathbf{a}$ are the velocity of water and air, respectively; $\mathbf{k}_\mathbf{w}$ and $\mathbf{k}_\mathbf{a}$ are permeability of water and air, respectively; h is total water head; γ_w is unit weight of water; and h_a is air pressure head. Permeability of water and air are expressed by Mualem's equation [5] and Van Genuchten's equation [6] as follows.

$$\mathbf{k}_\mathbf{w} = k_{rw}\mathbf{k}_\mathbf{wsat} = S_e^{1/2}\left[1 - \left(1 - S_e^{1/m}\right)^m\right]^2 \mathbf{k}_\mathbf{wsat} \tag{9}$$

$$\mathbf{k}_\mathbf{a} = k_{ra}\mathbf{k}_\mathbf{ares} = (1 - S_e)^{1/2}\left(1 - S_e^{1/m}\right)^{2m} \mathbf{k}_\mathbf{ares} \tag{10}$$

Here, k_{rw} and k_{rw} are the relative permeability of water and air, respectively; m is Mualem's coefficient; and $\mathbf{k}_\mathbf{wsat}$ and $\mathbf{k}_\mathbf{ares}$ are water permeability at a saturated state and air permeability at a perfectly dry state, respectively. The continuous equation of water and air are expressed by the application of three phases' mixture theory.

$$n\dot{S}_r - S_r\dot{\varepsilon}_v + \mathrm{div}\tilde{\mathbf{v}}_\mathbf{w} = 0 \tag{11}$$

$$(1 - S_r)\dot{\varepsilon}_v + n\dot{S}_r - n(1 - S_r)\frac{\dot{p}_a}{p_a + p_0} - \mathrm{div}\tilde{\mathbf{v}}_\mathbf{a} = 0 \tag{12}$$

Here, n is porosity; ε_v is volumetric strain; and p_0 is atmospheric pressure. The elasto-plastic constitutive model can be obtained from equation (4) and the force equilibrium equation as follows.

$$\dot{\boldsymbol{\sigma}}' = \mathbf{D} : \dot{\boldsymbol{\varepsilon}} - \mathbf{C} \cdot \dot{S}_e \tag{13}$$

Here, $\mathbf{D}$ is the elasto-plastic stiffness matrix; $\boldsymbol{\varepsilon}$ is the strain increment tensor; and $\mathbf{C}$ is the tensor expressing change in stiffness due to desaturation. The soil/water/air coupled problem was formulated by equations (11), (12) and (13). The soil water retention characteristic curve (SWRCC), which demonstrates the relationship between suction and soil moisture, is dependent on suction history. This hysteresis influences compaction behavior. In this study, the SWRCC model proposed by Kawai et al. [7] was used.

4. ONE-DIMENSIONAL RAINFALL INFILTRATION SIMULATION

Tsuchida et al. studied air behavior within ground exposed to relatively small rainfall. In this study, rainfall intensity large enough to generate a wetting front was simulated. The soil parameters used for the simulation are summarized in Table 1, and the soil water retention characteristic curves are shown in Fig. 3. Here, a sandy soil commonly used for general earth structures was assumed. The analytical mesh shown in Fig. 3 was assumed in accordance with Tsuchida et al. The undrained water and undrained air boundaries were provided for right and left side boundaries. A flux boundary, corresponding to rainfall intensity, and a drained air boundary ($p_a = 0$) were applied to the upper

Table 1 Soil parameters used for simulation

λ	κ	M	p'_{sat} (kPa)	k_{wx} (m/h)	k_{wy} (m/h)	S_{ri}
0.087	0.009	1.375	1500	0.156	0.078	0.15
m	a	n	n_E	k_{ax} (m/h)	k_{ay} (m/h)	e_i
0.8	10	1.0	1.00	15.6	7.8	0.7

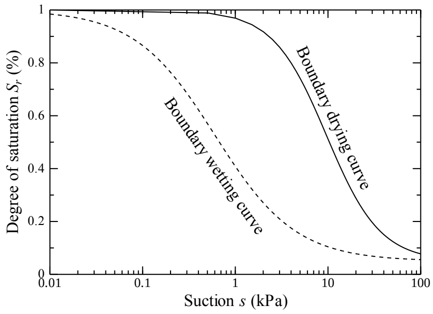

Fig. 3 Soil water retention characteristic curves

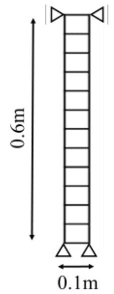

Fig. 4 Analytical mesh for one dimensional infiltration simulation

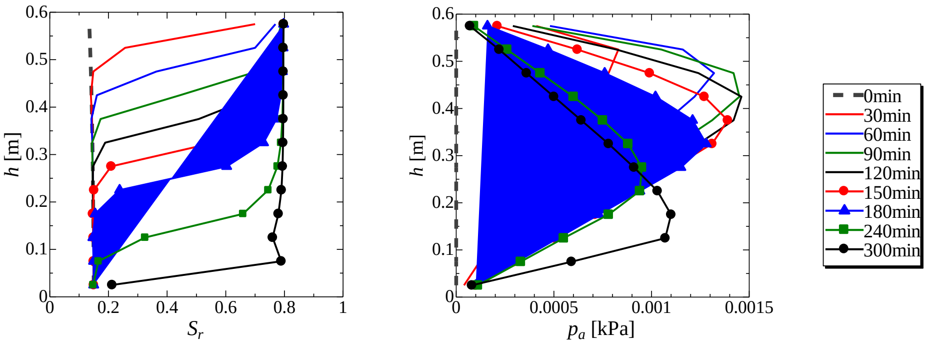

(a) Degree of saturation (b) Air pressure

Fig. 5 Rainfall intensity 30mm/h (Case DD)

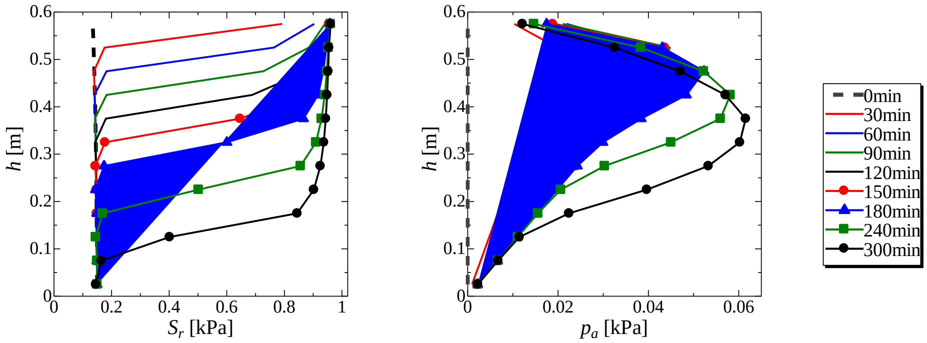

(a) Degree of saturation (b) Air pressure

Fig. 6 Rainfall intensity 60mm/h (Case DD) boundary. On the bottom of the analytical area, two kinds of boundary were investigated. One case, named Case DD, investigated the condition of drained air and drained water, using a value of $p_w = -5.5$(kPa) to indicate an initial distribution of suction. The other case, named Case UU, investigated undrained water and undrained air conditions. Rainfall intensities of 30 and 60 mm/h were simulated.

Figures 5 and 6 show the distribution of the degree of saturation and air pressure in Case DD. These results demonstrate that differences in infiltration behavior depended on rainfall intensity. Degree of saturation of the wetting front, indicating rainfall infiltration, was 0.8 for a rainfall intensity of 30mm/h, while it was over 0.9 for a rainfall intensity of 60mm/h. However, the time at which the degree of saturation started to increase at each depth was earlier for the 30mm/h than the 60mm/h rainfall intensity. This tendency can be explained due to the distribution of air pressure. The descent of the wetting front compressed air within the ground and increased the degree of saturation at the surface. Here, entrapment of air was more remarkable for the 60mm/h rainfall intensity, and compressed air prevented infiltrated water from descending. The wetting front for the 30mm/h rainfall intensity case exhibited a 0.8 degree of saturation, and air was easily exhausted from the surface. Consequently, air pressure gradually decreased after peaking at 90 minutes.

Figures 7 and 8 show simulation results obtained from Case UU. Because the bottom boundary was undrained water, infiltrated water accumulated here after the wetting front reached the bottom. Moreover, air pressure monotonically increased. In this case, the higher air pressure that was generated can predict a burst of compressed air from the ground surface.

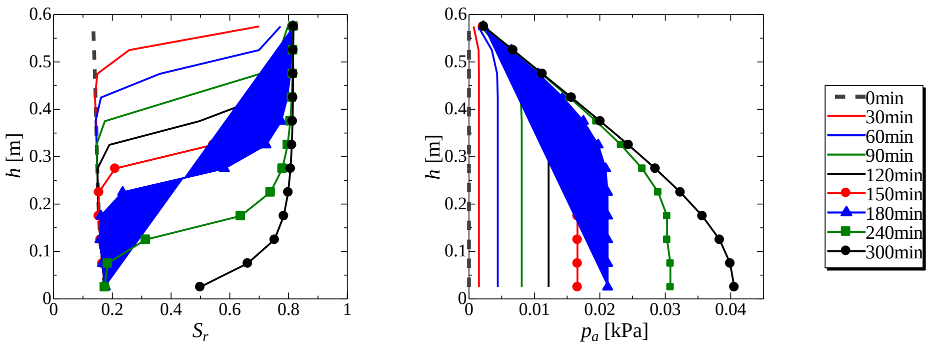

(a) Degree of saturation (b) Air pressure

Fig. 7 Rainfall intensity 30mm/h (Case UU)

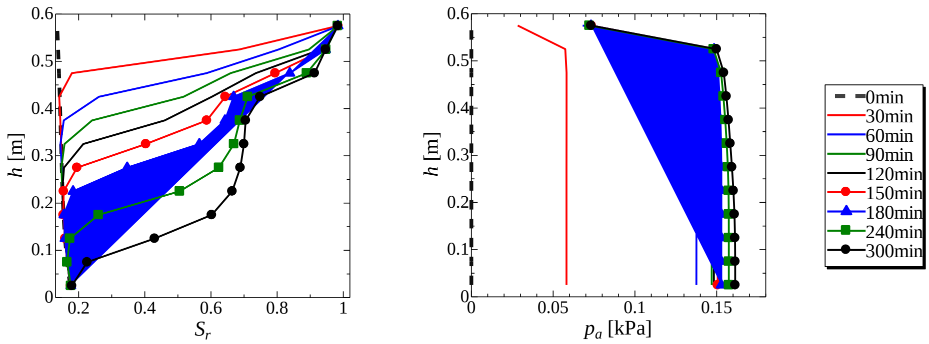

(a) Degree of saturation (b) Air pressure

Fig. 8 Rainfall intensity 60mm/h (Case UU)

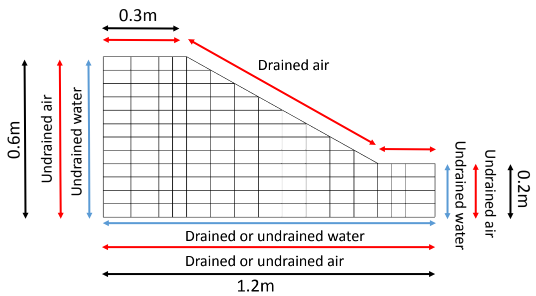

Fig. 9 Analytical mesh for rainfall simulation on sloping ground

5. RAINFALL INFILTRATION INTO SLOPING GROUND

On an actual slope, the direction of groundwater flow depends on slope shape. In this study, rainfall infiltration into sloping ground was simulated. Figure 9 shows the analytical mesh used in simulations. The right and left side boundaries were undrained water and air boundaries. The ground surfaces, including the crown and the slope, were both flux boundaries corresponding to rainfall intensity. The drainage condition of the bottom was changed with one-dimensional infiltration simulation. Input soil

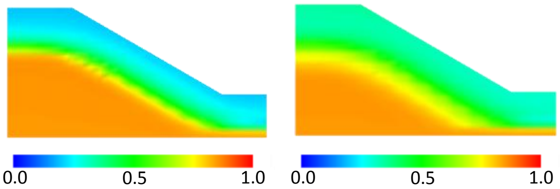

(a) 1.5 hour rainfall (b) 1 hour settling

Fig. 10 Degree of saturation (Case DD, 30mm/h)

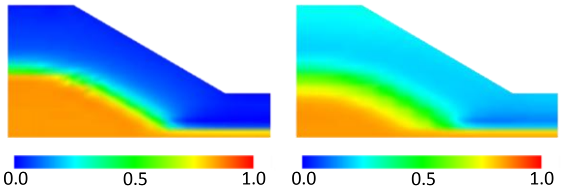

(a) 1.5 hour rainfall (b) 1 hour settling

Fig. 11 Degree of saturation (60mm/h, Case DD)

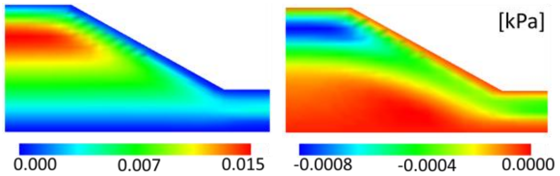

(a) 1.5 hour rainfall (b) 1 hour settling

Fig. 12 Air pressure (Case DD, 30mm/h)

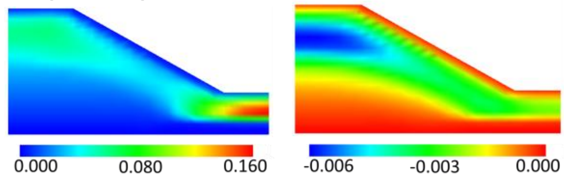

(a) 1.5 hour rainfall (b) 1 hour settling

Fig. 13 Air pressure (60mm/h, Case DD)

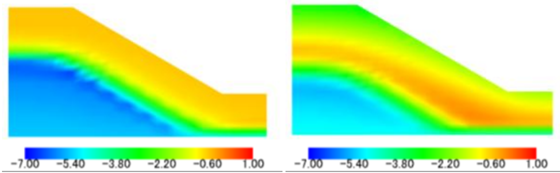

(a) 1.5 hour rainfall (b) 1 hour settling

Fig. 14 Water pressure (Case DD, 30mm/h)

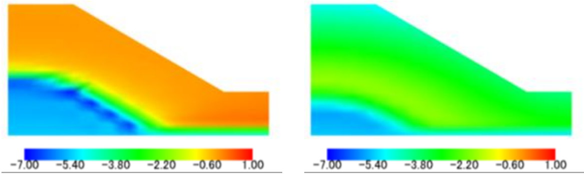

(a) 1.5 hour rainfall (b) 1 hour settling

Fig. 15 Water pressure (60mm/h, Case DD)

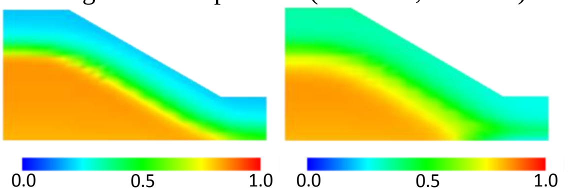

(a) 1.5 hour rainfall (b) 1 hour settling

Fig. 16 Degree of saturation (Case UU, 30mm/h)

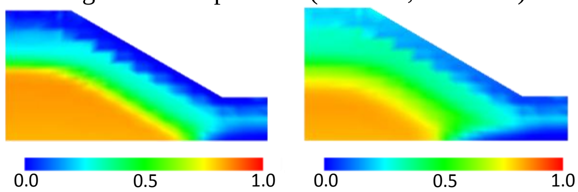

(a) 1.5 hour rainfall (b) 1 hour settling

Fig. 17 Degree of saturation (60mm/h, Case UU)

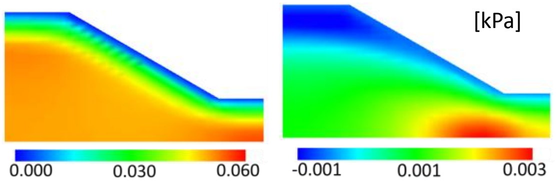

(a) 1.5 hour rainfall (b) 1 hour settling

Fig. 18 Air pressure (Case UU, 30mm/h)

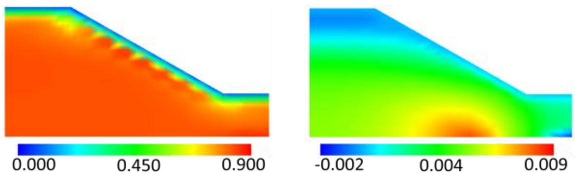

(a) 1.5 hour rainfall (b) 1 hour settling

Fig. 19 Air pressure (60mm/h, Case UU)

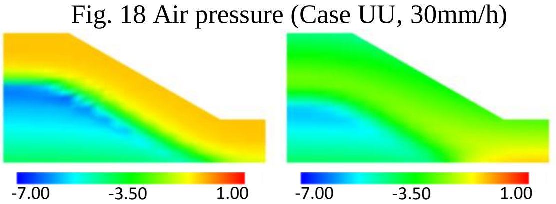

(a) 1.5 hour rainfall (b) 1 hour settling

Fig. 20 Water pressure (Case UU, 30mm/h)

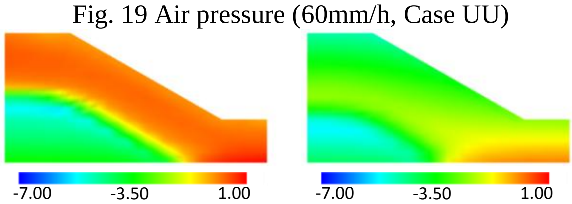

(a) 1.5 hour rainfall (b) 1 hour settling

Fig. 21 Water pressure (60mm/h, Case UU)

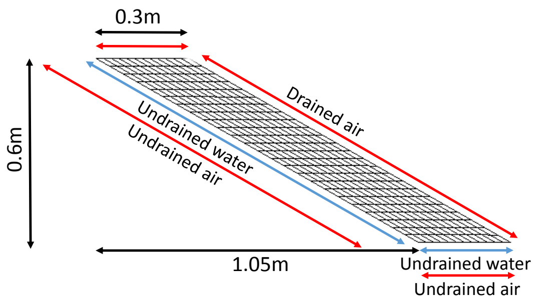

Fig22 Analytical mesh for rainfall simulation on sloping ground including weathered layer

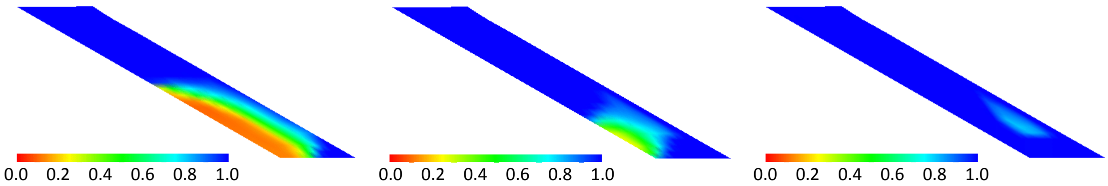

(a) 20min rainfall (b) 40min rainfall (c) 60min rainfall

Fig. 23 Degree of saturation

parameters are summarized in Table 1 and Fig. 3. Rainfall duration was 1.5 hour, and the settling time after rainfall is provided for each case.

Figures 10 and 11 show the distribution of the degree of saturation in the case of a drained bottom boundary (Case DD) under rainfall intensities of 30mm/h and 60mm/h, respectively. Rainfall of 60mm/h saturated the slope surface after 1.5 hours, while rainfall of 30mm/h did not saturate the surface in the same time period. Infiltrated water concentrated around the toe of slope during the settling term. This tendency was more remarkable for the higher rainfall intensity, shown in Fig. 11. This can be explained from equation (9). Unsaturated permeability depends on degree of saturation. Rainfall increases the degree of saturation around the slope surface first, resulting in an increase in the permeability around the slope surface. Consequently, flux parallel to slope becomes easier than vertical flux.

Figures 12 and 13 show the distribution of air pressure under rainfall intensities of 30mm/h and 60mm/h, respectively. An high air pressure area first appeared around the crown under a rainfall intensity of 30mm/h. This was because rainfall caused downward flux and pushed air toward the bottom as a drained boundary. Figures 14 and 15 show the distribution of water pressure. Rainfall increased the water pressure at the surface. However, the high water pressure area descended during the settling term, and negative water pressure appeared at the surface. This was because air permeability around the surface decreased due to saturation around the surface, and entrapped air expanded by downward flux. This led to negative air pressure around the crown. On the other hand, under a rainfall intensity of 60mm/h, since infiltrated water flowed parallel to the slope, the highest air pressure appeared around toe of slope.

Next, the same rainfall simulation was conducted under a condition of an undrained bottom boundary (Case UU). Figures 16 and 17 show the distribution of the degree of saturation under rainfall intensities of 30mm/h and 60mm/h, respectively. Since the bottom boundary was undrained, water infiltrating from the slope surface flowed towards the toe of slope and accumulated under the berm, especially under 60mm/h rainfall intensity. During the settling term, accumulated water spread to the left-hand side. However, in Case UU, the saturated area from the slope surface due to rainfall was smaller than in Case DD. This was because air was entrapped more easily and prevented rainfall from infiltrating. Figures 18 and 19 show the distribution of air pressure. In these figures, an area of high air pressure covered the whole of the sloping ground during rainfall, and it moved toward the toe of the slope during the settling term. This tendency was more remarkable and higher air pressure was generated under the higher rainfall intensity. Figures 20 and 21 show the distribution of water pressure. These results show that infiltrated water reached the bottom and tended to function as the phreatic surface.

Next, rainfall infiltration to sloping ground including weathered layer was simulated. In this case, bed layer is regarded as impermeable layer and the analytical mesh shown in Figure 22 was provided. Here, the bottom boundary was set up as undrained water and air boundary. Rainfall intensity was 60mm/h and rainfall term was 60mm. Figure 23 shows distribution of degree of

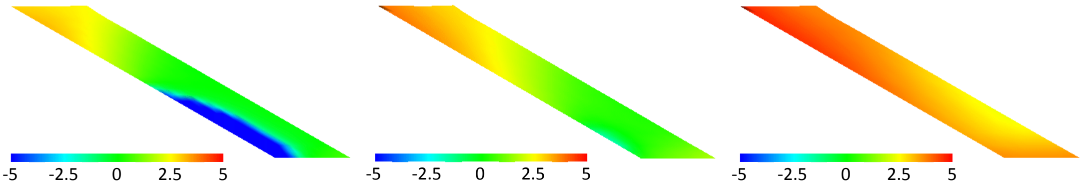

(a) 20min rainfall (b) 40min rainfall (c) 60min rainfall

Fig. 24 Water pressure

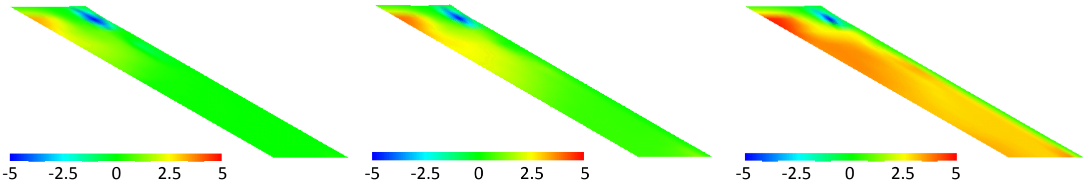

(a) 20min rainfall (b) 40min rainfall (c) 60min rainfall

Fig. 25 Air pressure

saturation. It is found that area around bed layer at the slope toe is saturated at last. Figures 24 and 25 show the distribution of water and air pressure, respectively. It is found that water and air pressure increased by rainfall around top of slope propagate toward slope toe.

6. CONCLUSIONS

In this study, rainfall infiltration was simulated with a soil/water/air coupled analysis to investigate rainfall effects on the behavior of air within the ground. Results show that the geometric condition and the drainage condition of water air strongly influenced the distribution of air pressure. Moreover, it was found that high pressure air entrapped by infiltrated water prevented rainfall from infiltrating. These results predict that compressed air will move towards a drained boundary and be finally exhausted. However, further considerations are needed to clarify the precursory phenomena of landslides.

7. REFERENCES

[1] Tsuchida, T., Yuri, A., Kano, S., Nakayabu, K., Yabuki, K., Hanaoka, N. & Kawabata, S. ‘Consideration of odor intensity within the ground and odor generation on landslide’, Journal of JGS, Vol.8, No.2, 2013, pp.339-348.

[2] Kanazawa, S. ‘Numerical evaluation of mechanical behavior of compacted soil structures based on a mathematical modelling for unsaturated soils’ Doctoral dissertation, Department of Civil Engineering, Kobe University, 2010 (in Japanese).

[3] Ohno S., Kawai K. & Tachibana S., ‘Elasto-plastic consti-tutive model for unsaturated soil applied effective degree of saturation as a parameter expressing stiffness’ Journal of JSCE, Vol. 63, No.4, 2007, pp.1132-1141 (in Japanese).

[4] Borja, R. I., ‘A mathematical framework for three-phase deformation and strain localization analysis of partially saturated porous media’ Computer methods in applied mechanics and engineering, Vol.193, 2004, pp.5301-5338.

[5] Mualem, Y., ‘A new model for predicting the hydraulic conductivity of unsaturated porous media’ Water Resources Research, Vol.12, No.3, 1976, pp.514-522.

[6] Van Genuchten, ‘A closed-form equation for predicting hydraulic of unsaturated soils’ Soil Science Society American Journal, Vol.44, 1980, pp.892-898.

[7] Kawai, K., Iizuka, A., Hayakawa, E. & Wang, W. ‘Non-uniform settlement of compacted earth structures caused by the deformation characteristics of unsaturated soil on wetting’ Soils and Foundations, Vol.47, No.2, 2007, pp. 195-206.